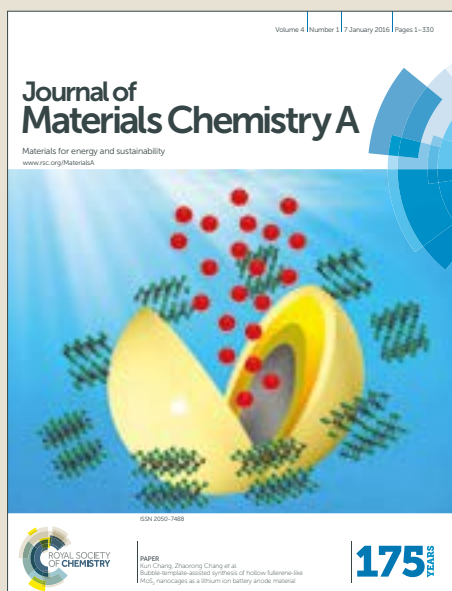


Journal of Materials Chemistry A

Accepted Manuscript



This article can be cited before page numbers have been issued, to do this please use: B. ren, D. li, Q. jin, H. cui and C. Wang, *J. Mater. Chem. A*, 2017, DOI: 10.1039/C7TA08090E.



This is an Accepted Manuscript, which has been through the Royal Society of Chemistry peer review process and has been accepted for publication.

Accepted Manuscripts are published online shortly after acceptance, before technical editing, formatting and proof reading. Using this free service, authors can make their results available to the community, in citable form, before we publish the edited article. We will replace this Accepted Manuscript with the edited and formatted Advance Article as soon as it is available.

You can find more information about Accepted Manuscripts in the [author guidelines](#).

Please note that technical editing may introduce minor changes to the text and/or graphics, which may alter content. The journal's standard [Terms & Conditions](#) and the ethical guidelines, outlined in our [author and reviewer resource centre](#), still apply. In no event shall the Royal Society of Chemistry be held responsible for any errors or omissions in this Accepted Manuscript or any consequences arising from the use of any information it contains.

Integrated 3D self-supported Ni decorated MoO₂ nanowires as highly efficient electrocatalysts for ultra-highly stable and large-current-density hydrogen evolution

Bowen Ren, Dongqi Li, Qiuyan Jin, Hao Cui,* and Chengxin Wang*

State Key Laboratory of Optoelectronic Materials and Technologies, School of Materials Science and Engineering, The Key Laboratory of Low-Carbon Chemistry & Energy Conservation of Guangdong Province, Sun Yat-Sen University, Guangzhou 510275, China

*Corresponding author: Fax: +86-20-8411-3901; e-mail: wchengx@mail.sysu.edu.cn; cuihao3@mail.sysu.edu.cn

KEYWORDS: nickel nanoparticles, molybdenum dioxide nanowires, 3D self-supposed, large current densities, hydrogen evolution reaction

ABSTRACT: The design and development of non-noble metal electrocatalysts for hydrogen evolution reaction (HER) is highly desirable, but still can not satisfy actual requirements in term of superior activity, ultrahigh stability and ability to carry large current densities. In this study, Ni nanoparticles anchored onto MoO₂ nanowires have been synthesized on carbon cloth via *in-situ* exsolution under reducing atmosphere. Impressively, the obtained Ni-MoO₂-450 NWs/CC exhibits excellent platinum-like HER activity with a nearly zero onset overpotential and a small Tafel slope of ~ 30 mV dec⁻¹, which implies the fast recombination step is rate-limiting.

Surprisingly, our sample gives an unprecedented stable catalytic activity over 320 hours in 1 M KOH, and can remain its activity at large current densities, even in the order of $1,000 \text{ mA cm}^{-2}$, which is far better than other reported catalysts. Such an outstanding performance should be mainly attributed to integrated 3D self-supposed nanocatalyst, high electronic conductivity framework and the synergistic coupling effect between Ni and MoO_2 interface. This work may thus provide an insight into the design and fabrication of alternative to Pt-based catalysts for the HER.

1. Introduction

Electrochemical splitting of water provides a simple and promising path to produce high-purity hydrogen as a storable and renewable chemical fuel. To prevent the adverse effect of acid fog, alkaline water splitting has been widely used for industrial hydrogen production.¹ However, it represents one of the biggest challenges in modern age on account of water splitting being an uphill reaction with a Gibbs free energy of $\Delta G = +237.2 \text{ KJ mol}^{-1}$, and the active electrocatalyst is essential to reduce the overpotential and advance electricity-to-hydrogen conversion efficiency, especially for the alkaline solution. As we all know, Pt-based metals are the most active hydrogen evolution reaction (HER) catalysts with negligible overpotentials and excellent kinetics for catalyzing the HER.^{2,3} Unfortunately, their unsatisfied stability in alkaline media, low earth abundance and rocketing cost seriously hinder large-scale applications.

Gratifyingly, great advances have been made in the development of efficient and low-cost HER electrocatalysts for the past few years.⁴⁻⁷ Nevertheless, under alkaline conditions, the performance still is much lower than that of Pt-based catalyst because of their sluggish kinetics reaction. Moreover, the most of current researches focus on the durability under small current

densities (e.g., at 10 mA cm⁻²) and short lasting time (e.g., less than 40 hours), which can not satisfy actual requirements at all.⁸

Considering all of the above-mentioned issues, the design and development of the state-of-the-art HER catalysts should satisfy multiple conditions simultaneously. (i) High activity with rapid kinetic reaction, (ii) Long-term stability more than 100 hours, and (iii) Affording large current densities as high as 1 A cm⁻² for practical commercial large-scale water electrolysis. In principle, the activity for the evolution of hydrogen is a function of the M-H (metal hydride) bond strength.⁹ M-H-strong metal is propitious to electrochemical reduction of H₂O into OH⁻ and intermediate H_{ads} (Volmer step), while M-H-weak metal facilitates the formation of intermediate H_{ads} into gaseous H₂ (Heyrovsky or Tafel step). Pt exhibits the superior activity with a moderate M-H bond strength, and its relatively low energy barrier of the Volmer step guarantees a fast Tafel step-determined HER process.⁵ Recently, researchers have successfully tailored various interfaces (such as MoS₂-Ni₃S₂, MoC-Mo₂C and Li⁺-Ni(OH)₂-Pt) with consequently facilitated HER kinetics.¹⁰⁻¹² It is a remarkable fact that HER is sensitive to the catalyst surface structure in alkaline media but largely insensitive in acids.¹⁰ Therefore, interface engineering may provide an effective strategy for designing HER catalysts with Pt-like kinetic mechanism in alkaline media. For stability, the catalysts should not only have high tolerance against corrosion, but also have a strong adhesion to the current collector to avoid peeling off during long-term electrocatalysis. Here, the design of the binder-free catalysts system is of great advantage and practical significance. In fact, the use of polymer binder could also block some catalytically active sites and further deteriorate the HER activity.¹³⁻¹⁵ For the third condition, the large current densities indicate rapid reaction rate of HER, which requires a high electronic conductivity to provide an easy access to the reactants and the electrons through the external circuit at the same time.⁸ The

common HER catalysts have the poor electronic conductivity, which could operate inefficiently at current densities as high as 1 A cm^{-2} .

Herein, we demonstrated Ni nanoparticles anchored onto MoO_2 nanowires grown on carbon cloth via *in-situ* exsolution under reducing atmosphere (denoted as Ni- MoO_2 NWs/CC). As a highly enhanced and stable electrocatalyst, it exhibits the following advantages: (1) The combination of Ni (M-H-weak) and Mo (M-H-strong) species may modify the electron density states of the d orbitals, thus change the M-H bond strength to an optimal value, which can provide a fast proton/electron-transfer step as well as a fast hydrogen release process like Pt, thus yields a synergism for the HER.¹⁶ (2) The 3D self-support structure with CC acting as a good current collector, not only offer more active sites but also can avoid catalyst peeling off during long-term electrocatalysis. (3) MoO_2 is a metallic semiconductor with a distorted rutile structure as Mo^{4+} in molybdenum oxides can cause an apparent metallic behavior.¹⁷ As a result, its low electrical resistivity ($8.8 \times 10^{-5} \text{ } \Omega \text{ cm}$) thus offer the good conductivity of the electrodes. Additionally, unlike the conventional impregnation method, the *in-situ* exsolution ensure abundant highly intimate interfaces between Ni and MoO_2 , which not only prevents the catalyst disintegration, but also minimizes the interfacial resistance between the hybrid species and provides the high electronic conductivity.¹⁸ As expected, it shows a zero onset overpotential and a low Tafel slope of $\sim 30 \text{ mV dec}^{-1}$. Notably, it gives an unprecedented stable catalytic activity over 320 hours in 1 M KOH (from 10 to 100 mA cm^{-2}), and its activity is well-remain at large current densities, even in the order of 1000 mA cm^{-2} .

2. Results and discussion

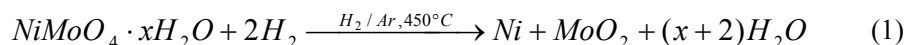
Ni-MoO₂ NWs were achieved on carbon cloth in two steps, as illustrated in **Scheme 1**. In the first step, Mo-Ni-O based precursors were grown by the hydrothermal process at 92 °C for 60 min. Then the color of the carbon cloth turned greyish-green from black gray (**Figure S1**, Supporting Information). As shown in **Figure S2** (Supporting Information), the carbon cloth substrate is fully covered by uniform nanowires (NWs) with an average diameter of about 80-150 nm, and average length of around 1 μm. Second, after the as-prepared precursors were annealed in a H₂/Ar (v/v, 1/1) atmosphere at 450 °C for 90 min, the color of the carbon cloth turned black and Ni-MoO₂-450 NWs/CC is obtained. Scanning electron microscopy (SEM, **Figure 1a**) image of Ni-MoO₂-450 NWs/CC shows that the original wire-like morphology is preserved. Compared with the smooth surfaces of Mo-Ni-O based precursors (**Figure S2d**, Supporting Information), numerous nanoparticles (NPs) are decorated uniformly on the surfaces of NWs (**Figure 1b**).

The XRD investigation clearly confirms the Ni-MoO₂-450 NWs/CC consists of cubic Ni (JCPDS 04-0850) and monoclinic MoO₂ (JCPDS 32-0671). As shown in **Figure 1c**, the peaks located at ~44.3° and 51.6° are indexed to (111) and (200) planes of Ni, respectively, peaks appearing at ~25.8°, 36.6°, 41.3°, 53.3°, and 66.2° are assigned to MoO₂. The XRD result reveals that the NWs are of the hybrid structure consisting of Ni and MoO₂. **Figure 1d-f** shows the XPS core-level spectra of Mo 3d, Ni 2p and O 1s for the Ni-MoO₂-450 NWs/CC. In Mo 3d region, the doublet at lower binding energy, Mo 3d_{5/2} (229.7 eV) and Mo 3d_{3/2} (232.9 eV), are characteristic of Mo⁴⁺.¹⁹ And the doublet at higher binding energy of Mo 3d_{5/2} and Mo 3d_{3/2} are assigned to Mo⁶⁺ specie, which resulted from surface oxidation upon air exposure.^{20,21} Additionally, the Mo 3d_{5/2} peak of Mo⁶⁺ is virtually in accordance with the Mo 3d_{3/2} peak of Mo⁴⁺, thus leading to the characteristic three-peak.²² In Ni 2p region, the Ni 2p_{3/2} peaks at 853.1

eV and the Ni $2p_{1/2}$ peaks at 870.4 eV are assigned to metallic Ni.²³ Two core-level peaks of Ni centered at 856.5 and 873.7 eV are ascribed to Ni²⁺ $2p_{3/2}$ and Ni²⁺ $2p_{1/2}$,²⁴ respectively, accompanying with two satellite peaks located at 862.5 and 880.7 eV.²⁵ In O 1s region, there is only one peak at 530.9 eV, which belongs to Mo-O species.

Transmission electron microscopy (TEM, **Figure 2a**) further demonstrated that NPs are homogeneously deposited on the surface of NW with the average diameter of 10-20 nm, in accordance with that suggested by SEM. High-resolution TEM (HRTEM, **Figure 2b**) indicate the clear lattice fringe with an interplanar distance of ~ 0.178 nm, which is assigned to the (200) plane of Ni. And the spacings of ~ 0.24 nm is assigned to MoO₂. Moreover, **Figure 2c** shows the corresponding selected area electron diffraction (SAED) patterns, and the diffraction rings are corresponding to (111) plane of Ni and some planes of MoO₂, confirming the co-existence of Ni and MoO₂. Noticeably, distribution of Mo, Ni and O elements are illustrated by energy-filtered TEM (EFTEM) mapping, Mo and O elements are mainly distributed in nanowire, while Ni element is mainly concentrated on nanoparticles. Obviously, all these results confirmed that Ni-MoO₂-450 NWs/CC consist of MoO₂ NWs modified by Ni NPs.

Additionally, different ambient atmosphere and annealing temperature are studied. When Mo-Ni-O based precursors were annealed at 400 °C in Ar atmosphere, NiMoO₄ (JCPDS 45-0142) NWs were obtained with the smooth surfaces (denoted as NiMoO₄NWs/CC, XRD pattern and SEM images are shown in **Figure S3**, Supporting Information). It suggests that H₂ is requisite to reduce the Mo-Ni-O based precursors into Ni and MoO₂. Specifically, the introduction of H₂ led to the formation of MoO₂ and inner Ni atoms gradually diffused outward, and Mo-Ni-O based precursors (NiMoO₄·xH₂O, **Figure S2e**) was transformed into Ni-MoO₂-450 NWs/CC via the following equation.



Therefore, the Ni NPs were constructed on the surfaces of MoO₂. After annealing at 350 °C in H₂/Ar atmosphere (denoted as Ni-MoO₂-350 NWs/CC), the morphology was basically retained (Figure S4a,b Supporting Information), while the crystallinity is deteriorated (Figure S4e, Supporting Information). When annealing at 550 °C in H₂/Ar atmosphere (denoted as Ni-MoO₂-550 NWs/CC), the morphology was still substantially maintained (Figure S4c,d, Supporting Information). However, MoNi alloy NPs were obtained instead of Ni NPs (Figure S4f, Supporting Information).

A typical three-electrode setup was employed to investigate the electrocatalytic HER activity of the electrocatalysts in Ar-saturated 1 M KOH aqueous solution at 25 °C. A graphite rod and a Hg/HgO electrode were used as the counter and reference electrodes, respectively. All the samples were subjected to electrochemical measurement without activation approaches, such as electrochemical activation. Figure 3a shows the polarization curves of Ni-MoO₂ NWs/CC annealed at different temperature. The carbon cloth and Pt foil (≥99.95% in purity) were also tested as reference. The Pt foil exhibit excellent catalytic activity with an onset potential of ~0 mV and requires the overpotential of 28 mV (η_{10}) to drive a current density of 10 mA cm⁻². As observed, the bare CC only shows a very poor current even when the potential is increased to -0.35 V vs RHE. Remarkably, Ni-MoO₂-450 NWs/CC exhibits the outstanding HER activity with a quite low onset potential of ~0 mV, which is comparable to that of the Pt foil. In addition, it needs small overpotentials of 40 and 49 mV to achieve current densities of -10 and -20 mA cm⁻² (η_{10} and η_{20}), respectively. Meanwhile, Ni-MoO₂-350 NWs/CC and Ni-MoO₂-550 NWs/CC give higher η_{10} of 56 and 55 mV, respectively. Noteworthy, when potentials continue to increase to exceed 57 mV, the performance of Ni-MoO₂-450 NWs/CC is even superior to that of Pt foil.

Figure 3c shows the polarization curve of Ni-MoO₂-450 NWs/CC under large overpotentials in comparison with Pt foil, it is noteworthy that Ni-MoO₂-450 NWs/CC shows superior activity with a η_{500} of 320 mV, indicating the remarkable catalytic ability for HER at large current densities. Based on the previous XRD results, the optimum interface structures (Ni and MoO₂) and crystallinity should be responsible for the excellent HER performance of Ni-MoO₂-450 NWs/CC and a summary of Ni-MoO₂ NWs/CC annealed at different temperature is listed in **Table S1** (Supporting Information).

The kinetic activities of the above electrodes are estimated by corresponding Tafel plots (**Figure 3b**). The Tafel slope of Ni-MoO₂-450 NWs/CC is only 30 mV dec⁻¹, which is far lower than those of Ni-MoO₂-350 NWs/CC (42 mV dec⁻¹) and Ni-MoO₂-550 NWs/CC (38 mV dec⁻¹), and is even competitive with that of Pt foil (28 mV dec⁻¹). The small Tafel slope suggests a fast increase of the hydrogen generation rate with the applied overpotential, corresponding to the high activity presented in the polarization curves. This result also indicates that the corresponding electrocatalytic HER kinetics of Ni-MoO₂-450 NWs/CC may determined by the Tafel step according to the classic theory, which is quite similar to that of Pt. All these observations demonstrate its catalytic activity is highly comparable to Pt, and is one of the state-of-the-art Pt-free HER electrocatalysts (**Table S2**, Supporting Information).

To have a deeper understanding of what the outstanding performance of Ni-MoO₂-450 NWs/CC originates from, ETH-Ni-MoO₂-450 NWs/CC was obtained by etching away Ni NPs from Ni-MoO₂-450 NWs/CC using HCl aqueous solution. As shown in **Figure S6** (Supporting Information), the Ni NPs were removed basically after etching. Apparently, ETH-Ni-MoO₂-450 NWs/CC shows a largely increased η_{10} of 318 mV, Tafel slope of 91 mV/dec, which are far higher than those of Ni-MoO₂-450 NWs/CC, as shown in **Figure 4a,b**. It indicates that Ni NPs is

indispensable for enhancing HER performance. In fact, it has been reported that Ni modification is a key factor to promote HER activity.^{26–28} For our material, it probably exhibits a synergistically-enhanced activity between Ni NPs and MoO₂ NWs. To reconfirm the possible synergistic effects, pure compact MoO₂ (CMP-MoO₂/CC), pure compact Ni (CMP-Ni/CC) and Ni coated compact MoO₂ (CMP-Ni-MoO₂/CC) were also synthesized (details in Experimental Section and **Figure S7** in Supporting Information). The CMP-Ni-MoO₂/CC exhibits an onset overpotential of 56 mV and needs η_{10} of 155 mV, η_{20} of 181 mV to approach 10 and 20 mA cm⁻², respectively. In sharp contrast, both CMP-MoO₂/CC and CMP-Ni/CC display much inferior HER activity with larger onset overpotentials of 234 and 132 mV, respectively. And CMP-MoO₂/CC and CMP-Ni/CC demand larger η_{10} of 338 and 265 mV, respectively, as shown in **Figure 4a**. Xun Wang *et al.*²⁸ have proposed the synergistic coupling effect between Ni and molybdenum carbide is attributed to the electron transfer from molybdenum carbide to neighboring Ni atoms. For Ni and MoO₂, they may follow similar kinetic processes. In other words, MoO₂ served as electron donor and Mo atoms generated more positive charge. As intermediate H_{ads} also possessed positive charge, the more positive charge Mo atoms generated, the weaker strength of M-H bond was. As previously mentioned, Mo (M-H-strong) species is propitious to Volmer step, but difficult to support Heyrovsky or Tafel step. Thus, the Mo atoms which generated more positive charge may decrease M-H bond strength to an optimal value, and in turn facilitate the desorptions of H_{ads} and H₂ release as well as Volmer step. Therefore, the synergistic coupling effect between Ni and MoO₂ interface can effectively speed up the rates of overall HER reactions. In addition, the exchange current density (j_0) was then extrapolated from the Tafel plots (**Figure S8**, Supporting Information), which represents the electrochemical reaction rate at equilibrium and is regarded as the most inherent measure of HER activity.^{6,29} As

expected, Ni-MoO₂-450 NWs/CC shows the highest j_0 of 5.0×10^{-1} mA cm⁻², which is far more than that of ETH-Ni-MoO₂-450 NWs/CC. And CMP-Ni-MoO₂/CC gives a j_0 of 1.6×10^{-1} mA cm⁻², which is obviously higher than those of CMP-MoO₂/CC and CMP-Ni/CC.

The origin of outstanding performance can also be deduced from the charge transfer resistance (R_{ct}) and electrochemical surface area (ECSA). Electrochemical impedance spectroscopy (EIS) spectra indicate that the R_{ct} of the Ni-MoO₂-450 NWs/CC (2.2 Ω) is smaller than that of ETH-Ni-MoO₂-450 NWs/CC (21.9 Ω), and the R_{ct} of the CMP-Ni-MoO₂/CC (102.3 Ω) is smaller than those of CMP-MoO₂/CC (806.2 Ω) and CMP-Ni/CC (231.9 Ω), as manifested by the diameter of the semicircle in **Figure 4c**. A smaller R_{ct} indicates the superior charge transport kinetics which benefits fast HER reaction. Besides, ECSA was further estimated by calculating the double-layer capacitances (C_{dl}) which are proportional to the ECSA values (**Figure S9**, Supporting Information).³⁰ As shown in **Figure 4d**, Ni-MoO₂-450 NWs/CC (242.0 mF cm⁻²) possessed a higher C_{dl} than that of ETH-Ni-MoO₂-450 NWs/CC (129.4 mF cm⁻²). And the C_{dl} of both CMP-MoO₂/CC (6.4 mF cm⁻²) and CMP-Ni/CC (3.0 mF cm⁻²) are lower than that of the CMP-Ni-MoO₂/CC (18.4 mF cm⁻²). A higher C_{dl} represents a larger active surface. The analyses of R_{ct} and ECSA imply that the introduction of Ni led to enhance HER activity by increasing reaction rate and enlarging active surface. A summary of the HER activity of the above materials is listed in **Table 1**.

Since we confirmed its outstanding performance, catalytic stability of Ni-MoO₂-450 NWs/CC was assessed by chronopotentiometry measurements. As the small current densities (e.g., at 10 mA cm⁻²) can not satisfy actual requirements for commercial industrial electrolyzers, the durability at large current densities is also an important criterion.^{8,31} **Figure 5a** shows chronopotentiometric curves obtained at multi-current-step conditions without replacing the

working electrode. The Ni-MoO₂-450 NWs/CC shows quite stable potentials throughout the current density change steps ranging from 10 mA cm⁻² to 100 mA cm⁻² for over 320 hours in total, which is the longest employed time reported so far. Remarkably, even under such harsh condition, the morphology and microstructure of Ni-MoO₂-450 NWs/CC keep unchanged, as demonstrated by the SEM and XRD images (**Figure 5b** and **Figure S10** in Supporting Information) after electrocatalysis. Further, considering the demands of practical application, the Chronopotentiometric curve was recorded at 500 and 1,000 mA cm⁻² (**Figure 5c**, without *iR* correction) in 30 wt% KOH solution (usual electrolyte in industrial alkaline electrolyzers). Surprisingly, the catalytic activity is well retained over 40 hours with barely any degrades in potential. Additionally, chronopotentiometric measurement was also performed in 1 M KOH (**Figure S11** in Supporting Information, without *iR* correction), the catalytic activity is well retained over 20 hours at 500 mA cm⁻². Even for 1,000 mA cm⁻² in 1 M KOH, the sample still exhibited the surprising stability with only 18% decay during 23 hours. All these observations demonstrate the Ni-MoO₂-450 NWs/CC possess the excellent platinum-like HER activity and superior stability, even at large current densities in alkaline medium.

The enhanced HER activity and stability of Ni-MoO₂-450 NWs/CC should be attributed to the following reasons, (a) the direct preparation of the catalyst on the carbon cloth substrate without using polymer binder or conducting agents, ensuring an intimate electrical contact and rapid electron transport^{32,33} and preventing catalyst from peeling off; (b) the 3D NWs configuration promotes the release of gas bubbles, enhancing the contact between electrolyte and active sites,^{34,35} and retarding the disintegration tendency of the electrode caused by rapid detachments of bubbles³⁶; (c) the conductive MoO₂ NWs could provide a much faster electron transfer during

the electrochemical reaction and afford large current densities; (d) the synergistic effect of Ni and MoO₂ may optimize the intrinsic electric properties of hybrids.

3. Conclusion

In summary, Ni NPs anchored onto MoO₂ NWs have been synthesized on carbon cloth through a simple hydrothermal reaction and a subsequent thermal annealing process. Compared with the electrocatalyst without Ni, the Ni-MoO₂-450 NWs/CC shows greatly enhanced electrocatalytic performances with a zero onset overpotential, a tiny overpotential of 40 mV at 10 mA cm⁻², and a low Tafel slope of ~30 mV dec⁻¹. Such activity even exceeds that of Pt at high overpotentials. Moreover, it affords a long-time steady catalytic output even at large current densities as high as 1A cm⁻². The enhanced property may be mainly ascribed to an optimized electron density, integrated 3D construction and high electronic conductivity framework, which consequently facilitates HER kinetics. This work provides a promising alternative to Pt catalysts and paves an exciting way for applications in the fields of energy conversion and storage.

4. Experimental Section

Materials: All chemicals were used without further purification. Nickel nitrate hexahydrate (Ni(NO₃)₂·6H₂O), sodium molybdate dihydrate (Na₂MoO₄·2H₂O) and molybdenum trioxide (MO₃) were purchased from Aladdin Ltd; Potassium hydroxide (KOH) and hydrochloric acid (HCl) were bought from Guangzhou Chemical Reagent Factory.

Synthesis of Ni-MoO₂ NWs/CC: Prior to the synthesis, a piece of carbon cloth (1 cm × 3 cm) was ultrasonically cleaned by acetone, ethanol, and deionized water in sequence. Typically, 1.57 mmol Ni(NO₃)₂·6H₂O and 1.57 mmol Na₂MoO₄·2H₂O were dispersed in 35 mL ethanol-water

solution with a volume ratio of 2:8 at room temperature to form a uniform solution. Subsequently, the cleaned carbon cloth was immersed into the above solution and transferred into a 50 mL Teflon-lined stainless steel autoclave. The autoclave was heated to 92 °C in an electric oven, kept for 60 min and then allowed to cooled down to the room temperature. Afterward, the carbon cloth with precursor was annealed at 350-550 °C for 90 min in a gas flow of 100 sccm Ar and 100 sccm H₂, with a pressure of 0.01 MPa. Finally, Ni nanoparticles anchored onto MoO₂ nanowires were obtained.

Synthesis of pure compact MoO₂/CC (CMP-MoO₂/CC): Typically, MO₃ powder with a purity of 99.8% was put in an alumina boat, and then, the cleaned carbon cloth was placed on the boat. Subsequently, it was quickly heated from room temperature to 750 °C (20 °C/min), and maintained at this temperature for 5 min. When the tube furnace was cooled to room temperature, the carbon cloth coated with MoO_x (CMP-MoO_x/CC) was obtained as precursor. Finally, CMP-MoO_x/CC was annealed at 450 °C for 90 min in a gas flow of 100 sccm Ar and 100 sccm H₂, with a pressure of 0.01 MPa.

Synthesis of pure compact Ni/CC (CMP-Ni/CC): The CMP-Ni/CC was prepared via an electrodeposition method using a three-electrode configuration with CC, a graphite rod, and Ag/AgCl as working electrode, counter electrode, and reference electrode, respectively. And 0.1 M NiSO₄·7H₂O was used as deposition solution. The electrodeposition process was performed by cyclic voltammetry for 30 cycles between -0.2 V and -1.4 V at a scan rate of 50 mV s⁻¹.²⁶ After deposition, the obtained sample was annealed under the same condition with CMP-MoO₂/CC.

Synthesis of Ni coated compact MoO₂ (CMP-Ni-MoO₂/CC): The CMP-Ni-MoO₂/CC was achieved using similar method to CMP-Ni/CC but using CMP-MoO_x/CC as working electrode.

Characterization: The surface morphologies of prepared samples were investigated by using of a scanning electron microscopy (SEM, Carl Zeiss, Auriga-4525) at an acceleration voltage of 5 kV. Transmission electron microscopy (TEM) images were taken using a FEI Tecnai G2 F30 microscope operated at 300 kV. X-ray photoelectron spectroscopy (XPS) were recorded by an ESCA Lab250 spectrometer using a twin-anode Al K α (1486.6 eV) X-ray source. The structural phases of the products were measured by powder X-ray diffraction experiments on a Rigaku X-ray diffractometer (D-MAX 2200 VPC) at 40 kV and 30 mA.

Electrochemical Measurements: All the electrochemical measurements were carried out at room temperature (298K) using an Autolab Potentiostat-Galvanostat connected to a standard three-electrode setup, with a hydrogen-saturated electrolyte solution. Because Pt can be dissolved and redeposited onto working electrode,³⁷ a graphite rod was used as the counter electrode. The Hg/HgO was chosen as the reference electrodes in 1M KOH. All potentials were calibrated with respect to the reversible hydrogen electrode (RHE) and iR-compensated by Electrochemical impedance spectroscopy (EIS) unless additional clarification. EIS was performed at the overpotential of 100 mV, in the frequency range of 10⁵ to 0.05 Hz with an amplitude of 10 mV.

ASSOCIATED CONTENT

Supporting Information.

Electronic supplementary information (ESI) available.

Conflicts of interest

The authors declare no competing financial interest.

Acknowledgements

This work was financially supported by the National Natural Science Foundation of China (Grants Nos. 51472276, 51772338 and U1401241). Pearl River S&T Nova Program of Guangzhou (Grant Nos. 201610010085). Guangdong special support program (Grant No. 2014TQ01C483).

AUTHOR INFORMATION

Corresponding Author

*E-mail: cuihao3@mail.sysu.edu.cn;

*E-mail: wchengx@mail.sysu.edu.cn

REFERENCES

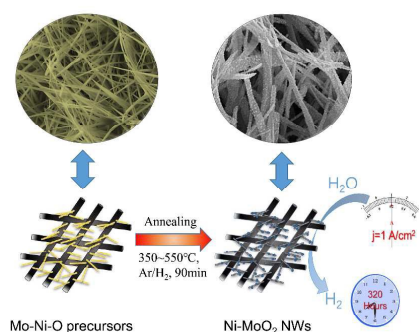
- 1 J.-X. Feng, H. Xu, Y.-T. Dong, X.-F. Lu, Y.-X. Tong and G.-R. Li, *Angew. Chem. Int. Ed.*, 2017, **56**, 2960–2964.
- 2 T. R. Cook, D. K. Dogutan, S. Y. Reece, Y. Surendranath, T. S. Teets and D. G. Nocera, *Chem. Rev.*, 2010, **110**, 6474–6502.
- 3 M. Wang, L. Chen and L. Sun, *Energy Environ. Sci.*, 2012, **5**, 6763–6778.
- 4 D. Li, Q. Liao, B. Ren, Q. Jin, H. Cui and C. Wang, *J Mater Chem A*, 2017, **5**, 11301–11308.
- 5 J. Zhang, T. Wang, P. Liu, Z. Liao, S. Liu, X. Zhuang, M. Chen, E. Zschech and X. Feng, *Nat. Commun.*, 2017, **8**, 15437.
- 6 B. Ren, D. Li, Q. Jin, H. Cui and C. Wang, *J Mater Chem A*, 2017, **5**, 13196–13203.
- 7 C. Tang, R. Zhang, W. Lu, L. He, X. Jiang, A. M. Asiri and X. Sun, *Adv. Mater.*, 2017, **29**, 1602441.
- 8 X. Zou, Y. Liu, G.-D. Li, Y. Wu, D.-P. Liu, W. Li, H.-W. Li, D. Wang, Y. Zhang and X. Zou, *Adv. Mater.*, 2017, **29**, 1700404.
- 9 Y. Zhang, B. Ouyang, J. Xu, S. Chen, R. S. Rawat and H. J. Fan, *Adv. Energy Mater.*, 2016, **6**, 1600221.
- 10 R. Subbaraman, D. Tripkovic, D. Strmcnik, K.-C. Chang, M. Uchimura, A. P. Paulikas, V. Stamenkovic and N. M. Markovic, *Science*, 2011, **334**, 1256–1260.
- 11 J. Zhang, T. Wang, D. Pohl, B. Rellinghaus, R. Dong, S. Liu, X. Zhuang and X. Feng, *Angew. Chem. Int. Ed.*, 2016, **55**, 6702–6707.
- 12 H. Lin, Z. Shi, S. He, X. Yu, S. Wang, Q. Gao and Y. Tang, *Chem Sci*, 2016, **7**, 3399–3405.
- 13 J. D. Roy-Mayhew, G. Boschloo, A. Hagfeldt and I. A. Aksay, *ACS Appl. Mater. Interfaces*, 2012, **4**, 2794–2800.
- 14 Y. Luo, J. Jiang, W. Zhou, H. Yang, J. Luo, X. Qi, H. Zhang, D. Y. W. Yu, C. M. Li and T. Yu, *J. Mater. Chem.*, 2012, **22**, 8634.
- 15 J. Shi, Z. Pu, Q. Liu, A. M. Asiri, J. Hu and X. Sun, *Electrochimica Acta*, 2015, **154**, 345–351.
- 16 Y.-Y. Ma, C.-X. Wu, X.-J. Feng, H.-Q. Tan, L.-K. Yan, Y. Liu, Z.-H. Kang, E.-B. Wang and Y.-G. Li, *Energy Environ. Sci.*, 2017, **10**, 788–798.
- 17 V. Eyert, R. Horny, K. Höck and S. Horn, *J. Phys. Condens. Matter*, 2000, **12**, 4923.
- 18 Y.-F. Sun, Y.-Q. Zhang, J. Chen, J.-H. Li, Y.-T. Zhu, Y.-M. Zeng, B. S. Amirkhiz, J. Li, B. Hua and J.-L. Luo, *Nano Lett.*, 2016, **16**, 5303–5309.
- 19 J. Jia, W. Zhou, G. Li, L. Yang, Z. Wei, L. Cao, Y. Wu, K. Zhou and S. Chen, *ACS Appl. Mater. Interfaces*, 2017, **9**, 8041–8046.
- 20 C. Wan, Y. N. Regmi and B. M. Leonard, *Angew. Chem. Int. Ed.*, 2014, **53**, 6407–6410.
- 21 H. Vrubel and X. Hu, *Angew. Chem. Int. Ed.*, 2012, **51**, 12703–12706.
- 22 Y. Jin and P. K. Shen, *J Mater Chem A*, 2015, **3**, 20080–20085.
- 23 M. Jiang, Y. Li, Z. Lu, X. Sun and X. Duan, *Inorg. Chem. Front.*, 2016, **3**, 630–634.
- 24 B. Zhang, C. Xiao, S. Xie, J. Liang, X. Chen and Y. Tang, *Chem. Mater.*, 2016, **28**, 6934–6941.
- 25 A. Mansour, *Surf. Sci. Spectra*, 1994, **3**, 231–238.
- 26 Z. Xing, D. Wang, Q. Li, A. M. Asiri and X. Sun, *Electrochimica Acta*, 2016, **210**, 729–733.
- 27 Y.-F. Xu, M.-R. Gao, Y.-R. Zheng, J. Jiang and S.-H. Yu, *Angew. Chem. Int. Ed.*, 2013, **52**, 8546–8550.
- 28 X. Xu, F. Nosheen and X. Wang, *Chem. Mater.*, 2016, **28**, 6313–6320.

- 29 A. T. Garcia-Esparza, D. Cha, Y. Ou, J. Kubota, K. Domen and K. Takanebe, *ChemSusChem*, 2013, **6**, 168–181.
- 30 M.-R. Gao, M. K. Y. Chan and Y. Sun, *Nat. Commun.*, 2015, **6**, 7493.
- 31 L. Zhu, H. Lin, Y. Li, F. Liao, Y. Lifshitz, M. Sheng, S.-T. Lee and M. Shao, *Nat. Commun.*, 2016, **7**, 12272.
- 32 L.-L. Feng, G. Yu, Y. Wu, G.-D. Li, H. Li, Y. Sun, T. Asefa, W. Chen, X. Zou and others, *J Am Chem Soc*, 2015, **137**, 14023–14026.
- 33 B. Ren, D. Li, Q. Jin, H. Cui and C. Wang, *J Mater Chem A*, 2017, **5**, 19072–19078.
- 34 D. Li, Q. Liao, B. Ren, Q. Jin, H. Cui and C. Wang, *J Mater Chem A*, 2017, **5**, 11301–11308.
- 35 Q. Jin, B. Ren, D. Li, H. Cui and C. Wang, *ACS Appl. Mater. Interfaces*, 2017, **9**, 31913–31921.
- 36 Xu-Dong Wang, Y.-F. Xu, H.-S. Rao, W.-J. Xu, H.-Y. Chen, W.-X. Zhang, D.-B. Kuang and C.-Y. Su, *Energy Env. Sci*, 2016, **9**, 1468–1475.
- 37 M. B. Stevens, L. J. Enman, A. S. Batchellor, M. R. Cosby, A. E. Vise, C. D. M. Trang and S. W. Boettcher, *Chem. Mater.*, 2017, **29**, 120–140.

BRIEFS

Ni nanoparticles anchored onto MoO₂ nanowires are achieved on carbon cloth as highly active and ultrastable electrocatalysts for hydrogen evolution. It gives excellent platinum-like HER activity and unprecedented stable catalytic activity over 320 hours even in the order of 1,000 mA cm⁻² in alkaline solution, which is far better than other reported catalysts.

SYNOPSIS



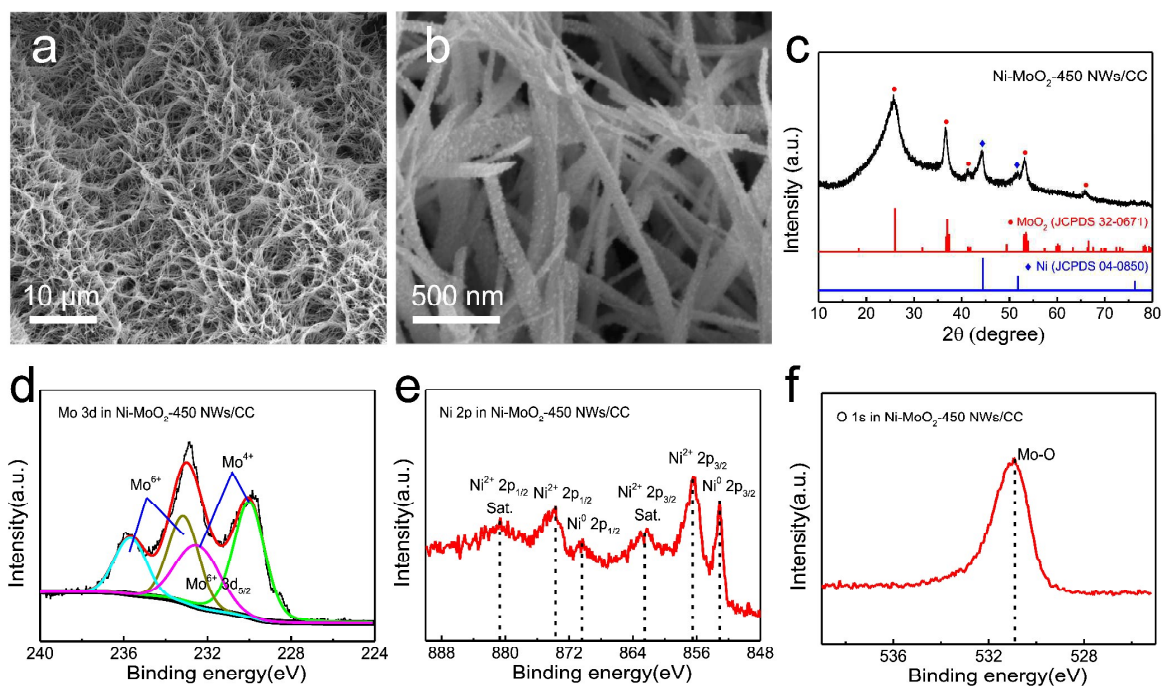


Figure 1. a) Low- and b) high-magnification SEM images of Ni-MoO₂-450 NWs/CC. c) XRD pattern of the Ni-MoO₂-450 NWs/CC with the standard crystallographic spectrum of Ni (JCPDS 04-0850) and MoO₂ (JCPDS 32-0671). XPS spectrum of Ni-MoO₂-450 NWs/CC for d) Mo 3d, e) Ni 2p and f) O 1s.

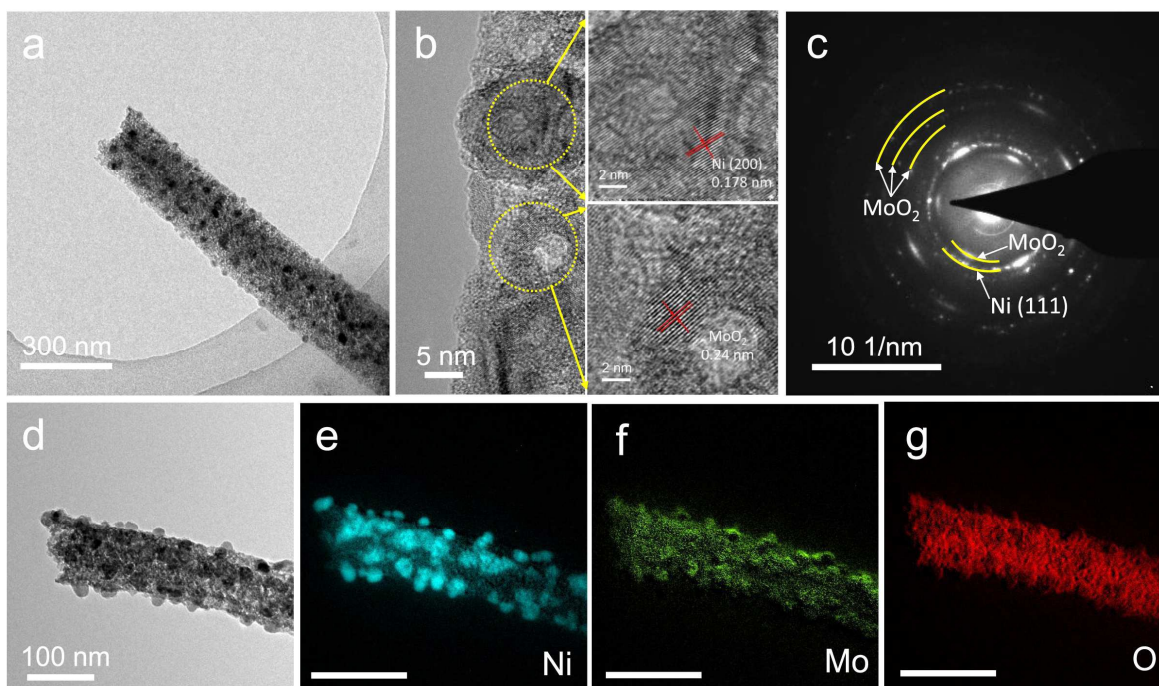


Figure 2. a) TEM and HRTEM image of Ni-MoO₂-450 NWs/CC. c) SAED pattern of the area shown in a). d) TEM image and corresponding EFTEM mapping of e) Ni, f) Mo and g) O element.

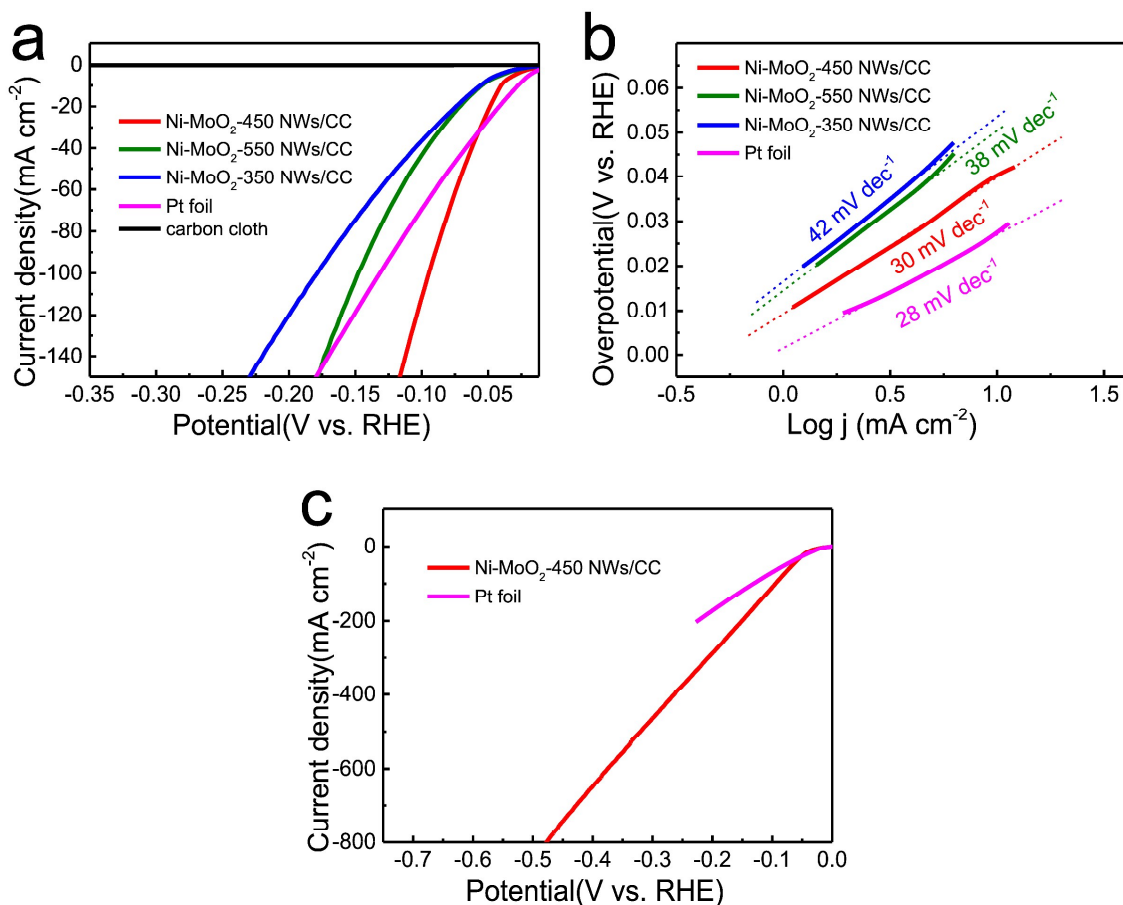


Figure 3. a) Polarization curves and b) Tafel plots of Pt foil and Ni-MoO₂ NWs/CC annealed at 350 °C, 450 °C and 550 °C in 1 M KOH, with a scan rate of 2 mV s⁻¹. c) Polarization curve of Ni-MoO₂-450 NWs/CC under large overpotentials, in comparison with Pt foil.

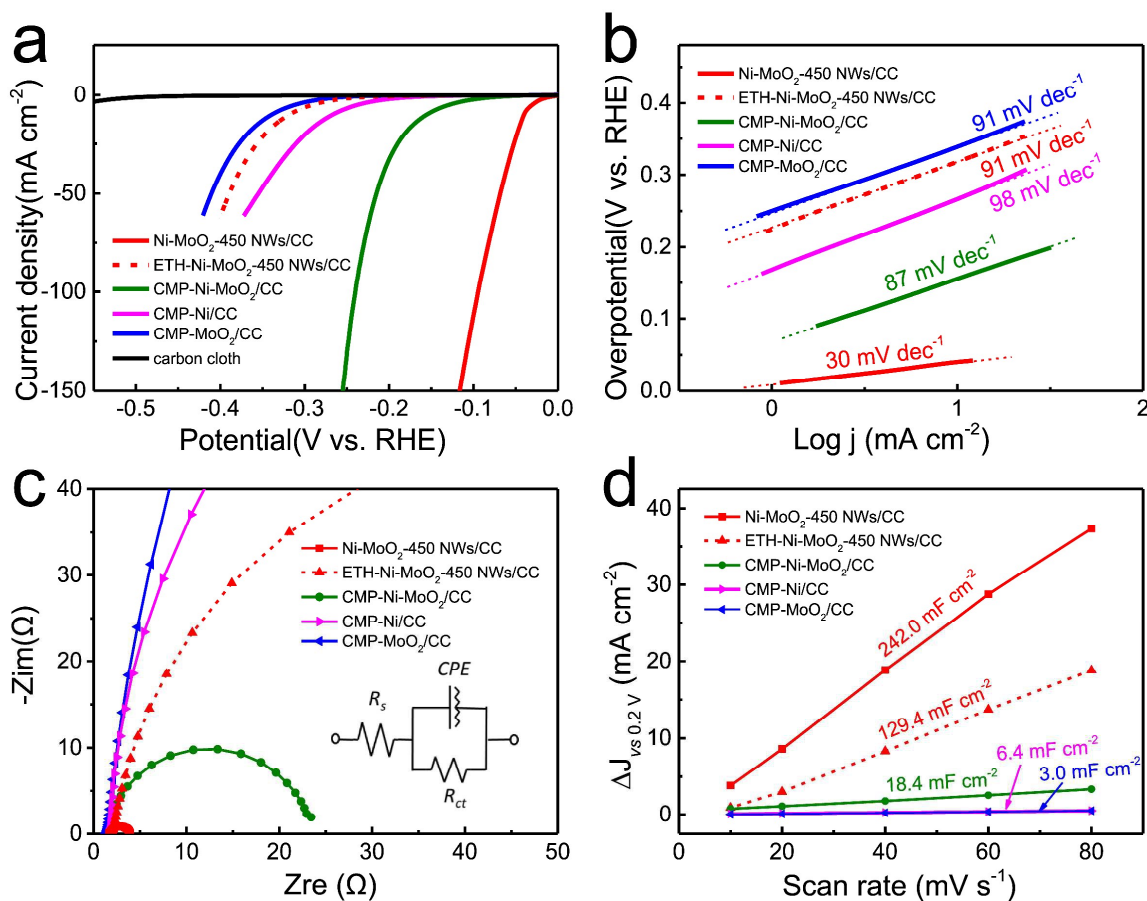


Figure 4. a) Polarization curves and b) Tafel plots of Ni-MoO₂-450 NWs/CC, ETH-Ni-MoO₂-450 NWs/CC, CMP-Ni-MoO₂/CC, CMP-MoO₂/CC, CMP-Ni/CC and carbon cloth in 1 M KOH, with a scan rate of 2 mV s⁻¹. c) Nyquist plots and d) Estimation of C_{dl} through plotting current density as a function of scan rate of the above electrocatalysts.

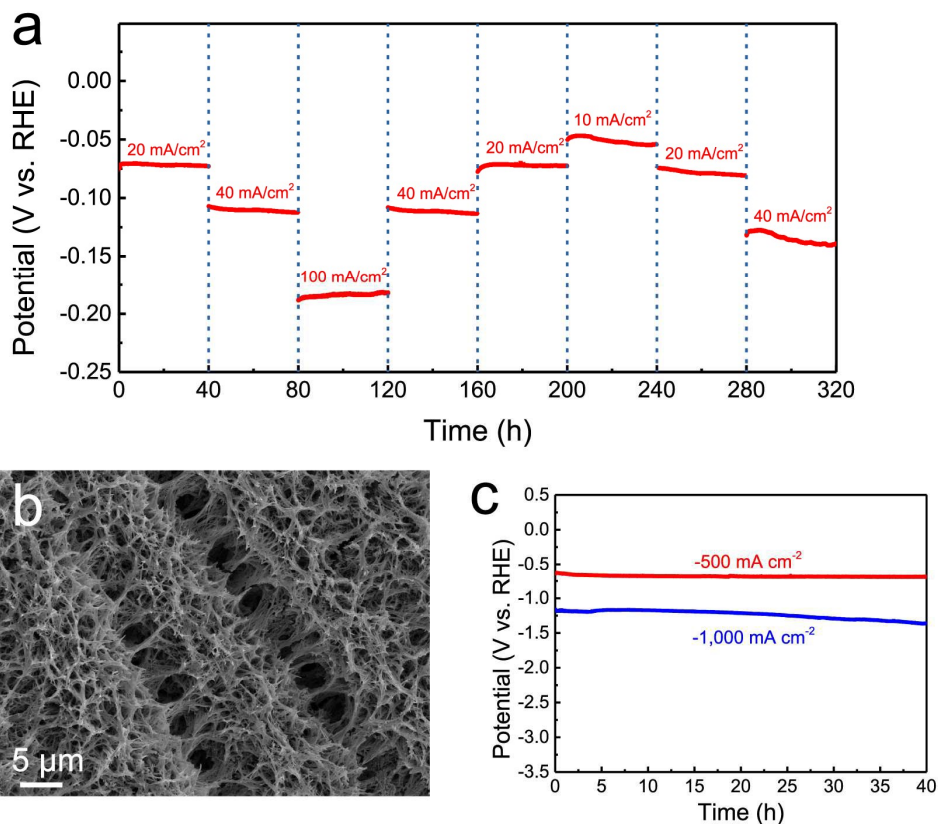


Figure 5. a) chronopotentiometric curves obtained at multi-current-step conditions (from 10 mA cm⁻² to 100 mA cm⁻²). b) SEM image of Ni-MoO₂-450 NWs/CC after the multi-current-step measurement. c) chronoamperometry measurement at a static current density of -1,000 mA cm⁻² for more than 40 hours without *iR* correction in 30 wt% KOH solution.

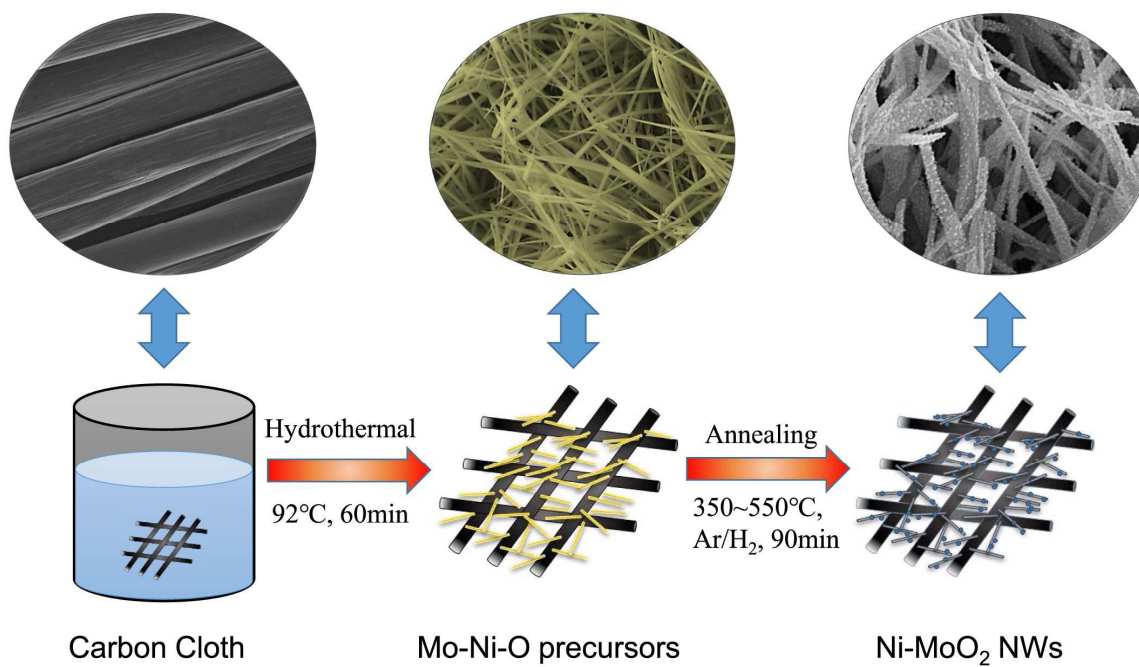
Scheme 1. A schematic of the fabrication process of Ni-MoO₂ NWs on a carbon cloth.

Table 1. Summary of the HER activity in 1 M KOH.

Materials	η_{10} (mV)	onset potential (mV)	Tafel slope (mV dec ⁻¹)	R_{ct} (Ω)	j_0 (mA cm ⁻²)	C_{dl} (mF cm ⁻²)
Ni-MoO ₂ -450 NWs/CC	40	0	30	2.2	5.0×10^{-1}	242.0
ETH-Ni-MoO ₂ -450 NWs/CC	318	221	91	21.9	3.3×10^{-3}	129.4
CMP-Ni-MoO ₂ /CC	155	56	87	102.3	1.6×10^{-1}	18.4
CMP-MoO ₂ /CC	338	234	91	806.2	1.9×10^{-3}	6.4
CMP-Ni/CC	265	132	98	231.9	1.9×10^{-2}	3.0